1    ***Staphylococcus aureus* skin colonization is mediated by SasG lectin variation**

2

3    Krista B. Mills[1], Joseph J. Maciag[2†], Can Wang[3†], John A. Crawford[4], Timothy J. Enroth[1], Klara

4    C. Keim[1], Yves F. Dufrêne[3], D. Ashley Robinson[4,5], Paul D. Fey[6], Andrew B. Herr[2,7,8], and

5    Alexander R. Horswill[1,9,*]

6    *[1]Department of Immunology and Microbiology, University of Colorado Anschutz Medical*

7    *Campus, Aurora, CO, USA*

8    *[2]Division of Immunobiology, Cincinnati Children's Hospital Medical Center, Cincinnati, OH, USA*

9    *[3]Louvain Institute of Biomolecular Science and Technology, UCLouvain, Louvain-la-Neuve,*

10   *Belgium*

11   *[4]Department of Cell and Molecular Biology, University of Mississippi Medical Center, Jackson,*

12   *MS, USA*

13   *[5]Center for Immunology and Microbial Research, University of Mississippi Medical Center,*

14   *Jackson, MS, USA*

15   *[6]Department of Pathology and Microbiology, University of Nebraska Medical Center, Omaha,*

16   *NE, USA*

17   *[7]Division of Infectious Diseases, Cincinnati Children's Hospital Medical Center, Cincinnati, OH,*

18   *USA*

19   *[8]Department of Pediatrics, University of Cincinnati College of Medicine, Cincinnati, OH, USA*

20   *[9]Department of Veterans Affairs, VA Eastern Colorado Healthcare System, Aurora, CO, USA*

21   [†]Contributed equally.

22   *Corresponding author. A. R. Horswill is to be contacted at the Department of Immunology and

23   Microbiology, 1635 Aurora Ct, Aurora, CO 80045, USA. Tel: 303-724-3534. *Email address:*

24   *alexander.horswill@cuanschutz.edu* (A.R. Horswill).

25

## Abstract

*Staphylococcus aureus* causes the majority of skin and soft tissue infections, but this pathogen only transiently colonizes healthy skin. However, this transient skin exposure enables *S. aureus* to transition to infection. Initial adhesion of *S. aureus* to skin corneocytes is mediated by surface protein G (SasG). Here, phylogenetic analyses reveal the presence of two major divergent SasG alleles in *S. aureus*, SasG-I and SasG-II. Structural analyses of SasG-II identified a unique non-aromatic arginine in the binding pocket of the lectin subdomain that mediates adhesion to corneocytes. Atomic force microscopy and corneocyte adhesion assays indicated SasG-II can bind to a broader variety of ligands than SasG-I. Glycosidase treatment resulted in different binding profiles between SasG-I and SasG-II on skin cells. Additionally, SasG-mediated adhesion was recapitulated using differentiated N/TERT keratinocytes. Our findings indicate that SasG-II has evolved to adhere to multiple ligands, conferring a distinct advantage to *S. aureus* during skin colonization.

## Introduction

The opportunistic pathogen *Staphylococcus aureus* is a common asymptomatic colonizer in humans but is also the predominant cause of skin and soft tissue infections [1]. Approximately 20% of the human population are persistently colonized by *S. aureus,* most commonly in the anterior nares, while 30% are transiently colonized [2,3]. *S. aureus* infections usually occur in individuals already colonized [3,4]. Despite causing approximately 76% of skin and soft tissue infections [5], *S. aureus* only colonizes 5% or less of the skin of otherwise healthy adults [6]. A trifecta of intact barrier, immune system, and commensal microbiota maintain skin homeostasis and keep *S. aureus* colonization rates low. However, dysbiosis or breaks in the skin barrier can lead to increased colonization levels and subsequent infection [7-9]. When skin homeostasis is compromised, *S. aureus* can deploy virulence factors that enable immune evasion and tissue invasion, further exacerbating inflammation and disease [10-12]. Identifying the mechanisms by which *S. aureus* colonizes healthy skin could open avenues for therapeutic development to prevent and treat infection in colonized individuals.

*S. aureus* skin colonization begins with initial adhesion, which is mediated by various cell wall-anchored (CWA) proteins [11,13-15]. In particular, surface protein G (SasG) is known to be important in *S. aureus* adhesion to healthy human corneocytes on the skin [15-17], as well as adhesion to nasal epithelial cells and in biofilm formation [18,19]. SasG is a large sortase-anchored protein that is part of the G5-E repeat family of adhesins [11]. The structure of this protein consists of a N-terminal A domain encompassing an intrinsically disordered region and L-type lectin, a B domain with highly-conserved, serial B-repeats containing G5-repeat and E-spacer sub-domains [11,16,18], and a proline/glycine-rich stalk region extending to the C-terminus [20]. SasG is orthologous to accumulation-associated protein (Aap) in *S. epidermidis*, and SasG homologs are expressed in other species of staphylococci as well [15]. Similar to SasG, Aap has been found to be important in *S. epidermidis* adhesion to healthy human corneocytes [15,16].

65    Previous studies have elucidated the role of the A domain, specifically the L-type lectin

66    subdomain, in Aap and SasG-mediated adhesion to corneocytes on healthy human skin [15-17]. L-

67    type lectins exhibit glycan-binding specificity that can significantly vary depending on the lectin

68    [21]. While the specific ligand for Aap and SasG is still unknown, recent data has indicated the

69    ligand is most likely a glycoprotein. Roy et al. [15] demonstrated that healthy human skin

70    corneocytes treated with the glycosidases PNGase and O-Glycosidase significantly reduced *S.*

71    *epidermidis* adhesion, suggesting these glycan linkages are important for adhesion to the host

72    ligand. A glycan array performed by Maciag et al. [16] supported these data and found that the

73    highest-affinity hits for the Aap lectin included N-linked glycans containing Gal-GlcNAc

74    alternating repeats (poly-N-acetyllactosamine). Furthermore, Maciag et al. identified key

75    aromatic residues within the glycan-binding pockets of the Aap and SasG lectins, which likely

76    bind glycans through stacking interactions. These key aromatic residues are approximately in

77    the same structural position, Y580 for Aap and W392 for SasG, and mutation of these residues

78    to alanine abrogated binding of these lectins to N-acetyl-D-lactosamine and 3'-sialyl-N-

79    acetyllactosamine as determined via isothermal titration calorimetry (ITC) [16]. Similarly, pre-

80    incubating corneocytes from healthy human skin with purified lectins from Aap and SasG

81    significantly reduced adhesion of both *S. epidermidis* and *S. aureus*, while the mutated lectins

82    did not affect adhesion [16], demonstrating that Aap and SasG bind to the ligand via these key

83    residues in the lectin subdomain.

84    The ability of purified lectins from both Aap and SasG to bind lactosamine derivatives

85    and reduce adhesion of both *S. epidermidis* and *S. aureus* to corneocytes suggests these

86    species may compete for adhesion to the same ligand on healthy human skin. However, in a *S.*

87    *epidermidis*-dominated skin environment [22,23] that is hostile to *S. aureus*, much has yet to be

88    elucidated as to what makes SasG unique and able to establish a colonization niche. Here, we

89    use phylogenetic analyses to demonstrate the presence of two divergent allelic types of SasG,

4

90    with each type represented by full-length and truncated forms, within *S. aureus*. We

91    demonstrate that SasG-II is unique and may bind to multiple ligands, based on evidence that

92    includes the SasG-II lectin structure and a lectin alignment comparison to SasG-I, adhesion

93    studies on corneocytes from healthy human skin and immortalized N/TERT keratinocytes, and

94    nanoimaging of corneocytes using SasG-I and SasG-II *S. aureus* single cell probes.

## Results

**The SasG A domain is variable in *S. aureus*.** Variability in the repertoire of sortase-attached adhesins is common on the surface of *S. aureus* [24]. SasG in particular has been noted as having significant strain-level diversity in gene (*sasG*) presence, expression level, and function [18,25]. We realized that *S. aureus* strains expressing full-length SasG, such as well-known strains COL and 502a in clonal complex 8 (CC8) and CC5, and MW2 in CC1, have considerable divergence in the A domain sequence. Considering the SasG A domain has been recently linked to corneocyte adhesion [15,17], we reasoned that the sequence differences could impact *S. aureus* skin colonization.

Full-length SasG from MRSA strain COL has a lectin domain that is structurally similar to that of *S. epidermidis* Aap, as we recently reported [16]. We named this form of SasG as Type I or "SasG-I" hereafter. In contrast, the A domain lectin in MRSA strain MW2 is only 67.2% identical at the protein level. We named this form of SasG as Type II or "SasG-II" hereafter. The rest of the protein content in both full-length SasG forms is fairly similar with the B-repeat region containing G5 and E spacers and a C-terminal wall/membrane spanning region with a LPKTG sortase motif (**Fig. S1A**). In this initial analysis, we also determined that some strains encoding SasG-I had an intact A domain and a frameshift mutation at the start of the B-domain. This includes strains such as N315 [26] and LAC [19] that belong to USA100-related and USA300 lineages, respectively. We named this mutated form of SasG-I as "truncated SasG-I". Some strains with SasG-II also encode a truncated protein; however, this form occurs less frequently among *S. aureus* strains and was not investigated further.

Both the Aap and SasG-I lectins have a key active site aromatic residue that has been linked to glycan binding and corneocyte adhesion, which is Y580 in Aap and W392 in SasG-I [16]. Based on an alignment of the SasG-I and SasG-II lectins, this aromatic residue is missing in

6

119   SasG-II and is replaced with non-aromatics (**Fig. S1B**). Other secondary structure elements are

120   similar, as expected given that both adopt β-sandwich L-type lectin folds. Based on our previous

121   analysis of the SasG-I and Aap lectin structures [16], most of the key residues in the vicinity of the

122   glycan binding site (shortly after β17) are conserved between SasG-I and SasG-II, with one

123   important exception, as described below.

124

125   **Phylogenetic analyses reveal the depth of SasG variation.** Building on our preliminary

126   observations, we further investigated SasG variation using a phylogenetically diverse set of *S.*

127   *aureus* isolates for which whole genome sequences were available [27]. These 574 isolates

128   belonged to 39 clonal complexes (**Fig. 1A**). Among these isolates, SasG was represented by

129   three approximately evenly distributed groups: 191 full-length SasG, 194 truncated SasG, and

130   189 missing SasG. Phylogenetic analysis of the aligned full-length SasG sequences confirmed

131   that the species has two divergent allelic types with 99 inferred amino acid substitutions

132   between them (**Fig. 1C**, long branch separating the two types). Among the full-length SasG

133   sequences, there were 91 unique SasG sequences with 11 distinct amino acid lengths of

134   sequence that could be attributed to the B-repeat region. The individual B-repeats were exactly

135   128 amino acids in length, and 11 differently sized repeat arrays were detected among the full-

136   length SasG sequences. The distribution of B-repeats among the two full-length SasG types

137   was significantly different ($\chi^2$=57.3, df=10, *P*<0.0001), with a more even number of B-repeats

138   among the Type II isolates compared to the Type I isolates (**Fig. 1B**).

139   Different isolates of a given clonal complex always had the same SasG type. However,

140   at least four changes of SasG types are inferred based on parsimony analysis of the type

141   distribution on the *S. aureus* phylogeny. The two SasG types correlate perfectly with amino acid

142   polymorphisms in the L-type lectin binding region: W392 for SasG-I, and R394 for SasG-II.

143   Since polymorphisms in these alignment positions correlated perfectly with the full-length SasG

144    types, these 2 amino acids were used to type the truncated SasG sequences. This typing

145    allowed for an additional parsimony analysis that identified a minimum of 27 changes between a

146    predicted functional SasG (full-length or typed-truncated sequence) and a predicted

147    nonfunctional SasG (missing or untyped-truncated sequence). The clonal complexes CC5 and

148    CC8, which are clinically important [28-30], both encode SasG-I but CC5 has mostly full-length

149    forms and CC8 has mostly truncated forms. SasG-II is encoded by CC1 (such as MRSA strain

150    MW2), as well as CC15, CC22, CC59, CC72, and others. SasG-II in these CCs are mostly full-

151    length, although some strains do rarely harbor truncated SasG-II.

152

153    **The SasG-II lectin contains a unique non-aromatic residue in the glycan binding pocket.**

154    The crystal structure of SasG-II lectin was solved at 1.88 Å, revealing an overall architecture

155    that is nearly identical to the L-type lectin folds of SasG-I, Aap, and Pls [16,31] (**Fig. 2A**). Similar to

156    these related lectin domains, SasG-II has an atypical *trans* conformation of the central D241

157    residue, a structural $Ca^{2+}$ ion, and three relatively long loops at the top of the domain. However,

158    both Aap and SasG-I lectins feature a sharp bend in the main chain after strand β17 that

159    positions an aromatic residue at the base of the glycan binding pocket (i.e., Aap Y580 and

160    SasG-I W392) (**Fig. 2B**). In contrast, SasG-II fails to adopt the sharp bend at the end of β17,

161    which therefore positions the sidechain of R394 in approximately the same position as the

162    SasG-II main chain after the bend. The arginine at this position is actually conserved between

163    SasG-I and SasG-II, but the sharp bend in the main chain of SasG-I causes the equivalent

164    R391 to extend toward the top of the lectin domain, far from the binding pocket, and positions

165    W392 within the binding pocket instead (**Fig. 2C**). Likewise, the Q395 residue in SasG-II

166    (corresponding to W392 in SasG-I) points in the opposite direction to R394 in a region of the

167    protein that is highly solvent-exposed (**Fig. 2C**). It seems likely that SasG-I and Aap adopt the

168    sharp bend in the main chain after β17 to avoid exposure of the equivalent aromatic residues

169    (W392 or Y580) to solvent, which would be entropically unfavorable. Instead, the main chain

170   bend orients those aromatic residues toward the binding site pocket region, which is more

171   protected from solvent. As a result of these structural differences, SasG-II forms a surface

172   pocket similar to the other lectins' glycan binding sites but it does not contain an aromatic

173   residue that could form a stacking interaction with a glycan ligand (**Fig. 2D**).

174

175   **Multiparametric nanoimaging using single bacterial probes indicates SasG-II binds a**

176   **broader variety of ligands than SasG-I.** To compare SasG-I and SasG-II-mediated adhesion

177   at the single molecule level and further explore the possibility of SasG-II binding multiple

178   ligands, we determined the strength of adhesion between a single living bacterial cell and

179   human corneocytes using multiparametric atomic force microscopy (AFM) imaging [32]. Bacterial

180   cells not expressing SasG (*S. carnosus*-pALC2073 EV) did not show any adhesion (**Fig. 3**),

181   similar to a colloidal probe (**Fig. 3 and Fig. S2**). Bacterial cells expressing SasG-II (*S. carnosus-*

182   *sasG*$_{MW2}$) showed strong adhesion forces ranging from 500 to 5,000 pN, with a most frequently

183   observed force of around 1,000 pN, that were densely and widely distributed across the

184   corneocyte surface (**Fig. 3 and Fig. S3**). It is likely that the 1,000 pN force corresponds to a

185   single interaction, while larger forces represent multiple bonds, possibly of a different molecular

186   nature. The detection frequency of 27% demonstrates that the SasG-II ligand(s) are present at

187   high density. SasG-I-expressing cells also showed many adhesion forces around 1,000 pN, yet

188   with a much lower detection frequency of approximately 7% (**Fig. 3 and Fig. S4**). This indicates

189   that both adhesins strongly bind their skin ligands, yet SasG-II seems to bind a broader variety

190   of ligands.

191

192   **Purified glycans do not affect SasG-II-mediated adhesion to corneocytes.** As we have

193   shown previously, the Aap and SasG-I lectins were both able to bind purified N-acetyl-D-

194   lactosamine via ITC [16]. Using ITC, we investigated whether SasG-II would also bind N-acetyl-D-

195    lactosamine, and found that the SasG-II lectin did not bind (**Fig. S5A**). This was functionally

196    validated in a corneocyte adhesion assay, where pre-incubation with a serial 2-fold dilution of N-

197    acetyl-D-lactosamine ranging from 1000 µM to 62.5 µM did not affect SasG-II-expressing *S.*

198    *carnosus-sasG*$_{MW2}$ adhesion to corneocytes (**Fig. S5B and S5C**). Similarly, pre-incubation with

199    a serial 2-fold dilution of 3'-sialyl-N-acetyllactosamine ranging from 100 µM to 6.25 µM (10-fold

200    lower dilutions than was used with N-acetyl-D-lactosamine) did not affect SasG-II-expressing *S.*

201    *carnosus-sasG*$_{MW2}$ adhesion to corneocytes (**Fig. S5D and S5E**). In contrast, adhesion of

202    SasG-I-expressing *S. carnosus*/pALC2073-*sasG*$_{COL}$ was strongly inhibited by 125 µM N-acetyl-

203    D-lactosamine or by 12.5 µM 3'-sialyl-N-acetyllactosamine [16]. These data collectively suggest

204    that SasG-II is unique from Aap and SasG-I, in that it may bind distinct glycan ligands on the

205    corneocyte receptor, or perhaps that it binds the protein portion of the receptor without engaging

206    the glycan moieties.

207

208    **SasG-I and -II mediated adhesion to corneocytes shows differential responses upon**

209    **treatment with glycosidases.** To narrow down possible ligand configurations for SasG-I and

210    SasG-II and further investigate binding differences between the two types, corneocytes were

211    pre-incubated with glycosidases. Protein glycosylation has been postulated to be important for

212    epidermal differentiation, as well as desquamation, hydration, and adhesion/cohesion of the

213    stratum corneum [33,34]. The most common types of glycans found on healthy human skin are

214    variations of complex N-linked glycans and mucin-like core 1 and core 2 O-linked glycans [34-37].

215    Seven different glycosidases were tested, including endoglycosidases and exoglycosidases.

216    PNGase F (cleaves between the innermost GlcNAc and asparagine residues of high-mannose,

217    hybrid, and complex oligosaccharides), O-Glycosidase (catalyzes removal of Core 1 and 3 O-

218    linked disaccharides from glycoproteins), α1-2,3,6 Mannosidase (catalyzes the hydrolysis of

219    terminal, non-reducing α1-2, α1-3 and α1-6 linked mannose residues from oligosaccharides),

220    α1-3,4 Fucosidase (catalyzes the hydrolysis of terminal, non-reducing α1-3 and α1-4 linked

221    fucose residues from oligosaccharides and glycoproteins), β-*N*-Acetylglucosaminidase S

222    (catalyzes the hydrolysis of terminal, non-reducing β-N-Acetylglucosamine residues from

223    oligosaccharides), β1-4 Galactosidase S (catalyzes the hydrolysis of terminal, non-reducing β1-

224    4 linked galactose residues from oligosaccharides), and α2-3,6,8 Neuraminidase (catalyzes the

225    hydrolysis of α2-3, α2-6, and α2-8 linked sialic acid residues from glycoproteins and

226    oligosaccharides).

227        We predicted that SasG-I-mediated adhesion would be similar to our previous results

228    with Aap [15], and would be reduced upon glycosidase treatment with the endoglycosidases

229    PNGase F and O-Glycosidase, as well as α2-3,6,8 Neuraminidase, and the exoglycosidases

230    α1-3,4 Fucosidase and β1-4 Galactosidase S. Indeed, pre-incubation with all five of these

231    glycosidases resulted in significantly reduced adhesion of *S. carnosus-sasG*$_{COL}$ compared to

232    buffer controls, while the exoglycosidases α1-2,3,6 Mannosidase and β-*N*-

233    Acetylglucosaminidase S did not affect adhesion (**Fig. 4A-G**). This suggests that linkages

234    between the innermost GlcNAc and asparagine residues of oligosaccharides, as well as Core 1

235    and 3 *O*-linkages are important in SasG-I mediated adhesion, and that 5-*N*-acetylneuraminic

236    acid, fucose, and galactose may be important in the SasG-I ligand configuration.

237        Considering the inability of the SasG-II lectin to bind lactosamine (**Fig. S5A**), we

238    predicted that SasG-II may bind different terminal sugar residues on corneocytes than SasG-I.

239    Using the same corneocyte adhesion assay, only pre-incubation with β-*N*-

240    Acetylglucosaminidase S and β1-4 Galactosidase S resulted in a reduction of *S. carnosus-*

241    *sasG*$_{MW2}$ adhesion (**Fig. 4A-G**). This indicates that terminal β-*N*-acetylglucosamine and

242    galactose may be important in the SasG-II ligand configuration. The only glycosidase that

243    resulted in both reduced SasG-I and SasG-II adhesion was β1-4 Galactosidase S, suggesting

244    that galactose may be important in the configuration of a shared ligand between SasG-I and

245     SasG-II. These results further suggest that SasG-II binds a different type of glycan ligand than

246     SasG-I on the corneocyte receptor.

247

248     **SasG-II-mediated adhesion is mediated by the lectin subdomain and may bind the same**

249     **ligand as Aap and SasG-I.** To investigate the possibility of a shared ligand between SasG-I

250     and SasG-II, we sought to determine if purified lectins from Aap, SasG-I, and SasG-II could

251     cross-inhibit SasG-II-mediated adhesion to corneocytes. Pre-incubating/blocking corneocytes

252     from healthy human skin with 5 µM purified lectin domains from Aap, SasG-I, and SasG-II

253     significantly reduced SasG-II-expressing MRSA MW2 adhesion, while purified lectins with the

254     key residues mutated–Aap ∆Y580A and SasG-I ∆W392A–did not affect adhesion (**Fig. 5A and**

255     **5B**). We then investigated whether this would hold true in the model surrogate organism *S.*

256     *carnosus*, which does not natively adhere to corneocytes [17]. Expressing SasG in *S. carnosus*

257     acts as an ideal model for testing protein-specific adhesion since there are no other adhesins

258     that could affect corneocyte binding. Similar to *S. aureus*, adhesion of *S. carnosus* expressing

259     SasG-II on plasmid pALC2073 was significantly reduced when pre-incubated/blocked with

260     purified lectins from Aap and SasG-I, but was not affected by pre-incubation with Aap ∆Y580A

261     or SasG-I ∆W392A, validating the findings in *S. aureus* (**Fig. 5C and 5D**). These data suggest

262     that SasG-II may bind to the same host ligand as SasG-I and Aap. Alternatively, SasG-II could

263     be binding elsewhere on the corneocyte receptor, sterically blocking SasG-I and Aap from

264     binding.

265          We then investigated if purified SasG-II could cross-inhibit SasG-I and Aap-mediated

266     adhesion to corneocytes. Purification of Type II full-length and A-domain SasG from MRSA

267     MW2 was characterized previously [19]. Pre-incubation/blocking with 100 µg/mL purified A domain

268     and full-length SasG-II significantly reduced *S. epidermidis* adhesion to corneocytes (**Fig. 5E**

269     **and 5F**). Likewise, pre-incubation/blocking with 100 µg/mL purified A domain and full-length

270    SasG-II significantly reduced SasG-I-expressing *S. carnosus-sasG*$_{COL}$ adhesion to corneocytes

271    (**Fig. 5G and 5H**). These findings suggest that the SasG-II mode of binding to the corneocyte

272    receptor enables competition with staphylococci expressing Aap or SasG-I.

273

274    **SasG-I and SasG-II-mediated adhesion to differentiated N/TERT keratinocytes following**

275    **treatment with glycosidases suggests complex N-linked glycans and core 2 O-glycans**

276    **may be important for SasG-I and SasG-II binding.** Firstly, to validate the adhesion data seen

277    on corneocytes and explore whether SasG could be utilized for invasion, we utilized a live,

278    immortalized, N/TERT-2G keratinocyte cell culture model. N/TERT keratinocytes can undergo

279    terminal differentiation, allowing for the presence of multiple keratinocyte layers with a

280    desquamated stratum corneum. Terminally differentiated N/TERT keratinocytes with a stratum

281    corneum were incubated with *S. carnosus*-pALC2073 EV (negative control), SasG-I-expressing

282    *S. carnosus-sasG*$_{COL}$, SasG-II-expressing *S. carnosus-sasG*$_{MW2}$, and SasG-II-expressing *S.*

283    *carnosus* with the A domain deleted (*S. carnosus-sasG*$_{MW2ΔA}$) [17]. Similar to what was seen in the

284    corneocyte adhesion assays, both SasG-I and SasG-II-expressing *S. carnosus* strains adhered

285    significantly more to differentiated N/TERTs than the EV and SasG-II A domain mutant controls

286    (**Fig. 6A and 6B**). To determine if SasG could be used not only in initial adhesion to the stratum

287    corneum but also for adherence to the more basal, actively dividing keratinocyte layers, these

288    same strains were then tested for adhesion to an undifferentiated monolayer of N/TERT

289    keratinocytes. Conversely, none of the strains adhered differently in a statistically significant

290    manner (**Fig. 6C and 6D**). The difference in adhesion for SasG-I-expressing *S. carnosus-*

291    *sasG*$_{COL}$ and SasG-II-expressing *S. carnosus-sasG*$_{MW2}$ on differentiated vs undifferentiated

292    N/TERT keratinocytes is illustrated in **Fig. 6E**, where much lower adhesion is seen for both

293    strains in undifferentiated N/TERT keratinocytes than differentiated N/TERT keratinocytes

294    containing a stratum corneum. These data indicate SasG is utilized by *S. aureus* for initial

295    adhesion to the outermost layer of the skin to establish a colonization niche, but not to infiltrate

296    deeper layers of the epidermis.

297        With the understanding that the ligand(s) to SasG exist on the stratum corneum, we then

298    investigated whether the glycosidase treatment on corneocytes would reveal similar glycan

299    ligand targets on live cells. *S. carnosus-sasG*$_{MW2}$ and *S. carnosus-sasG*$_{COL}$ were tested for

300    adhesion to differentiated N/TERT keratinocytes following pre-incubation with glycosidases β-*N*-

301    Acetylglucosaminidase S and β1-4 Galactosidase S. Similar to the corneocyte data, treatment

302    with these two glycosidases reduced *S. carnosus-sasG*$_{MW2}$ adhesion to differentiated N/TERT

303    keratinocytes. Though not statistically significant, β-*N*-Acetylglucosaminidase S exhibited a

304    reduced adhesion trend for *S. carnosus-sasG*$_{MW2}$, and this reduction was greater than what was

305    seen for *S. carnosus-sasG*$_{COL}$ (**Fig. 6F**). β1-4 Galactosidase S reduced adhesion of both *S.*

306    *carnosus-sasG*$_{COL}$ and *S. carnosus-sasG*$_{MW2}$, and resulted in a statistically significant reduction

307    for *S. carnosus-sasG*$_{COL}$ (**Fig. 6G**). These data confirm what was observed on corneocytes that

308    galactose may be important in the configuration of a shared ligand between SasG-I and SasG-

309    II, and that β-*N*-Acetylglucosamine may be uniquely important to a separate SasG-II ligand

310    configuration. Terminal β1-4-linked galactose and β-*N*-acetylglucosamine are found within

311    hybrid N-linked glycans [34], consistent with our previous observations that Aap binds to N-

312    glycans from the glycan array and that PNGase F abrogates adhesion mediated via SasG-I or

313    Aap [16]. However, terminal β1-4-linked galactose and β-*N*-acetylglucosamine are also both found

314    in core 2 mucin-type O-glycans [38]. SasG-II may interact with this type of O-glycan structure,

315    which would be consistent with the data that SasG-II-mediated adhesion is insensitive to

316    treatment with PNGase F or O-glycosidase (O-glycosidase can cleave core 1 or core 3, but not

317    core 2, O-glycans) (**Fig. 4**) [39]. The glycome of healthy skin prominently features numerous N-

318    glycoforms containing lactosamine or sialyllactosamine as well as core 2 O-glycans [35,36].

319

## Discussion

320

321        With over 50% of bacterial infections becoming resistant to treatment [40], identifying novel

322    ways to prevent infection has never been more imperative. One of the human body's first

323    defense mechanisms against external hazards is the human skin [41]. *S. aureus* plays an

324    important role in the skin environment, causing the majority of skin and soft tissue infections [5]

325    and contributing to morbidity in diseases such as atopic dermatitis [42-44]. Recent studies have

326    emphasized the importance of CWA adhesins in establishing colonization of human skin

327    corneocytes, which comprise the outermost layer of the skin [13-18]. One of these adhesins–

328    SasG–is a multifactorial protein that shares structural and functional similarity to *S. epidermidis*

329    Aap and has been characterized to be important in adhesion to corneocytes from healthy

330    human skin [15-17]. In this study, we identified variation in SasG via phylogenetic analyses, and

331    investigated how this variation affects adhesion to healthy human skin using a multifaceted

332    approach.

333        Phylogenetic analyses using a curated data set of the complete genomes from 574 *S.*

334    *aureus* isolates revealed approximately a third of strains express a full-length form and another

335    third express a truncated form of SasG. SasG-I is more than twice as common as SasG-II

336    across the diverse clonal complexes of *S. aureus* examined here. Lastly, approximately a third

337    of *S. aureus* strains do not encode SasG. Fibronectin binding protein B was recently found to

338    important in healthy corneocyte interactions and might explain the ability of *S. aureus* to bind

339    without SasG [13]. SasG-II occurs in some of the earlier diverging clonal complexes, but also

340    occurs in more derived clonal complexes likely due to a historical recombination event; it is not

341    likely that the two allelic types could independently originate multiple times through mutation

342    alone due to the large number of specific differences that define the two types. The observation

343    that both allelic types of SasG exist in full-length and truncated forms in currently circulating

344    strains, may suggest that retaining this molecular and functional variation is beneficial to *S.*

345    *aureus* as a species. Thus, SasG may be a new candidate of balancing selection in *S. aureus*

346    and needs to be further investigated [45].

347        The SasG-II lectin shares 67.2% sequence identity with the SasG-I lectin. Although the

348    overall fold of SasG-II is similar to that of SasG-I and Aap lectin domains, the local architecture

349    in the vicinity of the glycan binding site differs in SasG-II. In particular, SasG-II lacks the

350    characteristic aromatic residue (Aap Y580 or SasG-I W392) in the floor of the glycan binding

351    pocket. These aromatic residues in Aap and SasG-I are presumed to form a stacking interaction

352    with a bound glycan ligand, based on the loss of binding for the Y580A and W392A mutants of

353    Aap and SasG-I, respectively [16]. Thus, SasG-II may show a loss of glycan binding or a change

354    in glycan specificity compared to Aap and SasG-I. Given their overall sequence and structural

355    similarity, we conjectured that SasG-II might bind the same ligand as Aap and SasG-I as well as

356    an additional ligand(s) not yet identified. Pre-incubating/blocking healthy human corneocytes

357    with purified lectins from SasG-I and Aap was able to cross-inhibit SasG-II-mediated adhesion

358    to corneocytes, and purified SasG-II was likewise able to cross-inhibit SasG-I and Aap-mediated

359    adhesion. However, unlike the SasG-I and Aap lectins, which were found to bind both *N*-acetyl-

360    D-lactosamine and 3'-sialyl-*N*-acetyllactosamine by Maciag et al. 2023 [16], the SasG-II lectin did

361    not bind *N*-acetyl-D-lactosamine via ITC in our study. This was confirmed via corneocyte

362    adhesion assays, where this purified glycan did not affect SasG-II-mediated adhesion to

363    corneocytes. This suggests that SasG-II may bind the same glycan ligand as SasG-I and Aap,

364    but may also bind elsewhere on the corneocyte receptor and occlude SasG-I and Aap from

365    binding their respective glycan ligand.

366        AFM nanoimaging of corneocyte cell surfaces demonstrated weaker and less frequent

367    adhesive interactions for SasG-I than for SasG-II, indicating that while both types strongly bind

368    the ligand present on corneocytes, SasG-II may bind a broader variety of ligands and/or another

369    glycan ligand on corneocytes. Additionally, pre-treatment of corneocytes with glycosidases

370    resulted in different binding profiles between SasG-I and SasG-II. SasG-I-mediated adhesion

371    was reduced by PNGase F, O-Glycosidase, α2-3,6,8 Neuraminidase, and the exoglycosidases

372    α1-3,4 Fucosidase and β1-4 Galactosidase S, matching our previous report with the structurally

373    similar *S. epidermidis* Aap [15].  In contrast, SasG-II-mediated adhesion was reduced by only β-*N*-

374    Acetylglucosaminidase S and β1-4 Galactosidase S. The only glycosidase that resulted in

375    reduced adhesion of both SasG types was β1-4 Galactosidase S, suggesting that galactose

376    may be an important terminal sugar residue in a shared ligand between SasG-I and SasG-II,

377    while β-*N*-acetylglucosamine may be important in a ligand unique to SasG-II. Differentiated

378    N/TERT keratinocytes treated with β-*N*-Acetylglucosaminidase S and β1-4 Galactosidase S

379    further confirmed the corneocyte glycosidase data. Although SasG-I and Aap interact with

380    complex N-glycan structures [16], SasG-II adhesion was unaffected by PNGase F, suggesting that

381    SasG-II may bind to a distinct type of glycan. A likely candidate would be a core 2 O-glycan;

382    these can contain terminal β1-4 galactose and β-*N*-acetylglucosamine [38] but are insensitive to

383    cleavage by O-glycosidase [39]. Interestingly, N-glycans containing lactosamine or

384    sialyllactosamine and core 2 O-glycans are both prevalent species in the healthy skin glycome

385    [35,36].

386         While we do not know the exact structural nature of the ligand on the corneocyte

387    receptor, our findings strongly suggest that the ligand(s) are expressed on desquamated,

388    terminally differentiated keratinocytes and not basal keratinocytes, both SasG-I and SasG-II are

389    likely to interact with a glycoprotein, and that SasG-II may also engage with a core 2 O-glycan

390    structure (**Fig. 7**). The findings presented here as well provide further knowledge that could be

391    used to therapeutically target and prevent *S. aureus* skin colonization for individuals at-risk for

392    *S. aureus* infection in a prophylactic manner, potentially eliminating the need for traditional

393    antibiotics that could contribute to further drug resistance in these individuals.

394

## Materials and methods

**SasG-I and SasG-II lectin alignment.** The lectin protein sequences of SasG-I (from MSSA 502a) and SasG-II (from MRSA MW2) were aligned using Clustal Omega 1.2.4 [46]. Sequence similarities, secondary structure elements, and relative accessibility were extracted with the Clustal Omega protein alignment and Type I/Type II lectin protein coordinates using the DSSP program in ESPript 3.0 [47].

**SasG phylogenetic analyses.** Variation in SasG was analyzed in the context of *S. aureus* phylogenetic diversity. In brief, a previously curated data set of complete genomes from 574 *S. aureus* isolates, and 1 *S. argenteus* isolate that served as an outgroup, was obtained from the PATRIC database [48-50]. PhyloPhlAn3 [51] was used to align conceptually translated protein sequences from the *S. aureus* proteome, curate the alignment, and perform phylogenetic analysis using default settings. Clonal complexes were identified on the phylogeny as clusters of related multilocus sequence types. SasG sequences were extracted from these proteomes and strains were sorted into three groups based on the state of their SasG sequence as full-length, truncated, or absent. Full-length SasG sequences were aligned with MUSCLE v3.8.31[52,53] and clustered with CD-HIT v4.8.1 [54,55] at 100% identity. Gblocks v0.91b [56] was used with stringent settings (min. seq. for flank pos.: 85%, max. contig. nonconserved pos.: 4, min. block length: 10, no gaps in final blocks) to remove alignment gaps, including the SasG B-repeat sequences. PhyML [57] was used with the WAG model to infer a SasG phylogeny and to define two SasG allelic types. Mesquite v3.70 [58] was used to perform parsimony analysis with the *S. aureus* phylogeny to reconstruct SasG presence/absence and SasG allelic type; since the parsimony analysis ignores branch lengths it was not necessary to account for recombination events on the *S. aureus* phylogeny for this analysis. The R statistics package was used to perform a chi-squared goodness-of-fit test of the B-repeat distributions of the two SasG allelic types.

420

421 **SasG-II lectin crystallography.** The SasG-II lectin domain was expressed as a fusion protein

422 with an N-terminal hexahistidine tag followed by a tobacco etch virus (TEV) protease site using

423 the pDest17-His plasmid in *E. coli* BLR (DE3) cells (Novagen). Protein expression and

424 purification was conducted as described for SasG-I lectin domain [16]. Crystals were grown via

425 hanging drop diffusion. Protein stocks were at a concentration of 10 mg/mL in 20 mM Tris-HCl

426 (pH 7.2) and 300 mM NaCl. Stocks were combined with mother liquor in equal parts (1 µL + 1

427 µL). Crystals appeared after five days in a condition of 100 mM HEPES (pH 7.8), 200 mM

428 Ammonium Sulfate, 25%-33% BCS PEG SMEAR Medium (Molecular Dimensions,

429 CalibreScientific). Cryoprotectant consisted of 80% mother liquor and 20% MPD; crystals were

430 plunged into cryoprotectant prior to being flash frozen in liquid nitrogen. Data collection occurred

431 at the Advanced Photon Source at Argonne National Lab through the Northeastern

432 Collaborative Access Team (NE-CAT) on the 24-ID-E beamline. Data sets were collected at an

433 oscillation range of 0.2°, collecting 900 frames, at a resolution range of 78.074-1.799 Å. Data

434 indexing, space group assignment, scaling, and integration were carried out in the CCP4i suite

435 [59]. Structure determination was carried out by PHENIX: PHASER using Aap lectin [16] as a search

436 model for molecular replacement and building the initial SasG-II model with PHENIX: Autobuild.

437 Iterative cycles of refinement and model building using data to a maximum resolution of 1.88 Å

438 were carried out using PHENIX [60] and Coot [61], respectively. The final refined model was

439 submitted for validation using MolProbity [62]. Data collection and refinement statistics for the

440 SasG-II lectin domain can be found in **Table S1**.

441

442 **Multiparametric imaging using single bacterial probes.** SasG-I-expressing *S. carnosus*-

443 SasG$_{COL}$, SasG-II-expressing *S. carnosus-sasG*$_{MW2}$, or *S. carnosus*-pALC2073 (EV) and a

444 healthy skin corneocyte (0.5 cm × 0.5 cm) were immobilized on two different and separate

445    areas on the bottom of a petri dish. The corneocyte was attached to one side of the petri dish

446    using a double-sided transparent tape. 50 µL of diluted bacterial suspension in phosphate-

447    buffered saline (PBS) was deposited on the other side of a Petri dish and allowed to adhere for

448    15 minutes at room temperature. The Petri dish was then carefully washed twice with PBS to

449    remove non-adhering cells, after which 3 mL of PBS buffer was added to perform atomic force

450    microscopy (AFM) experiments.

451    Single-cell probes were obtained by attaching a single bacterium to a colloidal probe.

452    Colloidal probes were prepared as elucidated previously [63]. Colloidal probe cantilevers were

453    immersed for 60 minutes in Tris-buffered saline (TBS; Tris, 50 mM; NaCl, 150 mM; pH 8.5)

454    containing 4 mg mL$^{-1}$ of dopamine hydrochloride (Sigma-Aldrich), rinsed in TBS, and used

455    directly for cell probe preparation. The nominal spring constant of the colloidal probe cantilever

456    was determined by the thermal noise method [64], giving an average value of ~0.06 N/m. The

457    colloidal probe was brought into contact with a single isolated bacterium to catch it via

458    electrostatic interaction with polydopamine and then moved on top of the corneocyte (kindly

459    provided by Prof. Joan Geoghegan); proper attachment of the cell on the colloidal probe was

460    checked using optical microscopy.

461    Multiparametric images of corneocytes were recorded in PBS using a bacterial probe

462    under the Quantitative Imaging™ mode available on the Nanowizard III and IV AFM (JPK

463    Instruments, Germany). Images were obtained using a *S. carnosus* cell probe on top of a

464    corneocyte at a scan area of 45 µm × 45 µm (256 pixels × 256 pixels), with an applied force of

465    0.5 nN, and a constant approach and retraction speed of 40 µm s$^{-1}$ (z-range of 1 mm). For each

466    condition, experiments were repeated for at least 3 different cell pairs.

467

468     **Isothermal titration calorimetry.** ITC experiments were performed as previously described [16]

469     using a MicroCal VP-ITC microcalorimeter. Analysis and fitting were done with ORIGIN

470     software. Sample cells contained 20 µM of lectin protein (1.5 mL) and the syringe contained 1

471     mM of glycan (450 µl). The heat response from twenty glycan injections was measured; the first

472     injection was a volume of 2 µl and the subsequent nineteen injections were at a volume of 14 µl

473     each.

474

475     **Corneocyte collection.** Desquamated corneocytes from the lower or upper arm near the elbow

476     were collected from healthy human volunteers, as described in Mills et al. 2022 [17]. Clear,

477     adhesive tape stripping discs (d-Squame D100; Clinical & Derm) were used to collect

478     corneocytes following cleaning and air-drying of the collection area with an alcohol wipe.

479

480     **Preparation of bacterial strains for corneocyte and N/TERT adhesion assays.** The bacterial

481     strains used in this study are listed in **Table S2**. Bacterial cultures were prepared as described

482     in Mills et al. 2022 [17]. All bacterial strains expressed superfolder green fluorescent protein

483     (sGFP), either on plasmid pCM29 for *S. aureus* and *S. epidermidis* strains or chromosomally for

484     *S. carnosus* strains. Strains were grown overnight at 37 °C with shaking aeration at 220 rpm in

485     tryptic soy broth (TSB) in the presence of 10 µg/mL of chloramphenicol for plasmid

486     maintenance. Strains were then sub-cultured at a 1:50 dilution in TSB with chloramphenicol and

487     grown to an OD600 of ~0.75. Strains were diluted to a final OD600 of 0.15 (~$10^7$ colony-forming

488     units [CFU]/mL) after washing once in PBS at a 1:1 ratio. An OD600 of 0.15 was chosen to

489     allow for adequate cell enumeration without clumping of bacterial cells [15,17].

490

491     **Corneocyte adhesion assays.** The corneocyte adhesion assays were performed as described

492     in Mills et al. 2022 [17].

493      ***Co-incubation with purified glycans.*** SasG-II-expressing *S. carnosus-sasG*$_{MW2}$ was

494      tested for adhesion to corneocytes following co-incubation with the purified glycans *N*-

495      acetyl-D-lactosamine (Sigma-Aldrich) or 3'-sialyl-*N*-acetyllactosamine (Sigma-Aldrich).

496      *N*-acetyl-D-lactosamine was prepared in PBS to a concentration of 1000 µM and diluted

497      2-fold from 1000 µM to 62.5 µM. 3'-Sialyl-*N*-acetyllactosamine was prepared in PBS to a

498      concentration of 100 µM and diluted 2-fold from 100 µM to 6.25 µM. 300 µL of prepared

499      glycans and 300 µL of prepared bacterial strains were co-incubated at room temperature

500      for 20 minutes. The entire 600 µL was then incubated on corneocytes for 45 minutes at

501      37 °C. *S. carnosus*-pALC2073 was used as a negative control.

502      ***Pre-incubation with glycosidases.*** *S. carnosus* strains expressing SasG-I (*S.*

503      *carnosus-sasG*$_{COL}$) and SasG-II (*S. carnosus-sasG*$_{MW2}$) were tested for adhesion to

504      corneocytes following deglycosylation. Corneocytes were incubated with one of the

505      following glycosidases for 24 hours at 37 °C in a moist chamber: PNGase F, O-

506      Glycosidase, α1-2,3,6 Mannosidase, α1-3,4 Fucosidase, β-*N*-Acetylglucosaminidase S,

507      β1-4 Galactosidase S, and α2-3,6,8 Neuraminidase (NEB). A 300 µL total solution for

508      each enzyme contained: 3 µL enzyme, 30 µL GlycoBuffer (specific to each enzyme),

509      and 30 µL BSA supplement for α1-3,4 Fucosidase or 30 µL zinc supplement for α1-2,3,6

510      Mannosidase, and addition of PBS up to 300 µL. After 24 hours, corneocytes were

511      washed with PBS and subsequently incubated with the specified strains for 45 minutes

512      at 37 °C. Each of the prepared solutions without the enzymes were used as control

513      conditions for each experimental group.

514      ***Pre-incubation/blocking with purified lectins.*** Strains with SasG-II, *S. aureus* MW2

515      and *S. carnosus*-SasG$_{MW2}$, were tested for adhesion to corneocytes following pre-

516      incubation/blocking with purified recombinant lectins from Aap, Aap ΔY580A, SasG-I,

517      SasG-I ΔW392A, and SasG-II. Protein purification of the lectins is described in Maciag et

518      al. 2023 [16]. Lectins were prepared to a concentration of 5 µM in 300 µL PBS. The

519 prepared lectins were incubated on corneocytes at room temperature for 20 minutes,

520 followed by incubation with 300 µL prepared bacterial strains for 45 minutes at 37 °C. *S.*

521 *aureus* Δ*mgrA* Δ*sasG* or *S. carnosus*-pALC2073 (EV) were used as negative controls.

522 ***Pre-incubation/blocking with purified Type II full-length SasG and SasG-II A-***

523 ***domain.*** This assay followed a similar procedure as described in Mills et al. 2022 [17]. *S.*

524 *epidermidis* and SasG-I-expressing *S. carnosus-sasG*$_{COL}$ were tested for adhesion to

525 corneocytes following pre-incubation with purified full-length SasG-II or purified A-

526 domain from *S. aureus* MW2. 300 µL of purified protein were prepared in PBS at a

527 concentration of 100 µg/mL and incubated on corneocytes for 45 minutes at room

528 temperature, followed by incubation with 300 µL prepared bacterial strains at 37 °C for

529 45 minutes. *S. epidermidis* Δ*ica* Δ*aap* or *S. carnosus*-pALC2073 (EV) were used as

530 negative controls.

531

532 **N/TERT adhesion assays.** To study the adhesion of SasG to live host cells, immortalized

533 N/TERT-2G keratinocytes were utilized [65]. Here, low passage (<10) undifferentiated N/TERT-2G

534 cells were seeded to $1 \times 10^5$ cells/mL in either experiment media (EM) [65] or keratinocyte serum-

535 free medium (KSFM, Gibco) in a 24-well tissue culture treated plate. For the assays on

536 differentiated N/TERT-2G cells, the keratinocytes were both seeded in and allowed to

537 differentiate in EM for 1 week with media changes every two days to promote the formation of a

538 stratified and thick layer of epithelial cells. For assays using undifferentiated N/TERT-2G cells,

539 cells were seeded in KSFM and were allowed form a 100% confluent monolayer (approximately

540 2-3 days growth) with daily media changes. All cells were grown at 37°C with 5% $CO_2$.

541 On the day of experimentation, cells were inoculated with *S. carnosus*-pALC2073 (EV),

542 *S. carnosus-sasG*$_{MW2}$ (SasG-II), *S. carnosus-sasG*$_{COL}$ (SasG-I), or *S. carnosus-sasG*$_{MW2ΔA}$

543 prepared in PBS. The growth media was removed, and each strain was inoculated onto

23

544    N/TERT-2G cells in technical triplicate at an MOI of 5 using a total inoculum volume of 100 uL.

545    Upon addition of bacteria, the bacteria were allowed to incubate on the cells for 30 minutes

546    following a 5-minute spin at 1000 rpm. After the 30-minute incubation, the N/TERT-2G cells

547    were gently washed three times with 500 uL of sterile PBS per well to remove any un-adhered

548    bacteria. 100 uL of 0.05% trypsin-EDTA (Sigma-Aldrich) was then added to each well and

549    allowed to incubate for 10 minutes at 37°C with 5% $CO_2$. The trypsinized cells were then

550    resuspended in 400 uL sterile PBS, serially diluted, and plated to quantify the bacterial CFU/mL.

551    Adhered bacterial cells were assessed as overall percent adhesion as well as percent cell

552    association normalized to the *S. carnosus*-*sasG*$_{MW2}$ input inoculum.

553        ***Pre-incubation with glycosidases.*** *S. carnosus* strains expressing SasG-I (*S.*

554    *carnosus*-*sasG*$_{COL}$) and SasG-II (*S. carnosus*-*sasG*$_{MW2}$) were tested for adhesion to

555    differentiated N/TERT-2G keratinocytes following deglycosylation. Cells were seeded and

556    allowed to differentiate for 1 week as described above. Cells were incubated with glycosidases

557    β-*N*-Acetylglucosaminidase S and β1-4 Galactosidase S at a 1:100 ratio in KSFM for 24 hours.

558    After incubation, the cells were inoculated with the *S. carnosus* strains and followed the same

559    adhesion and quantification protocol as described above.

# References

1. Parlet, C.P., Brown, M.M., and Horswill, A.R. (2019). Commensal Staphylococci Influence Staphylococcus aureus Skin Colonization and Disease. Trends Microbiol *27*, 497-507. 10.1016/j.tim.2019.01.008.

2. Brown, A.F., Leech, J.M., Rogers, T.R., and McLoughlin, R.M. (2014). Staphylococcus aureus Colonization: Modulation of Host Immune Response and Impact on Human Vaccine Design. Front Immunol *4*, 507. 10.3389/fimmu.2013.00507.

3. Otto, M. (2010). Staphylococcus colonization of the skin and antimicrobial peptides. Expert Rev Dermatol *5*, 183-195. 10.1586/edm.10.6.

4. von Eiff, C., Becker, K., Machka, K., Stammer, H., and Peters, G. (2001). Nasal carriage as a source of Staphylococcus aureus bacteremia. Study Group. N Engl J Med *344*, 11-16. 10.1056/NEJM200101043440102.

5. Moran, G.J., Krishnadasan, A., Gorwitz, R.J., Fosheim, G.E., McDougal, L.K., Carey, R.B., Talan, D.A., and Group, E.M.I.N.S. (2006). Methicillin-resistant S. aureus infections among patients in the emergency department. N Engl J Med *355*, 666-674. 10.1056/NEJMoa055356.

6. Leung, D.Y. (2003). Infection in atopic dermatitis. Curr Opin Pediatr *15*, 399-404. 10.1097/00008480-200308000-00008.

7. Bieber, T. (2020). Targeting T2 Inflammation by Dupilumab Impacts on the Microbiomic "Menage a Trois" of Atopic Dermatitis. J Invest Dermatol *140*, 15-17. 10.1016/j.jid.2019.07.680.

8. Brown, M.M., Kwiecinski, J.M., Cruz, L.M., Shahbandi, A., Todd, D.A., Cech, N.B., and Horswill, A.R. (2020). Novel Peptide from Commensal Staphylococcus simulans Blocks Methicillin-Resistant Staphylococcus aureus Quorum Sensing and Protects Host Skin from Damage. Antimicrob Agents Chemother *64*. 10.1128/AAC.00172-20.

9. Lee, S.M., Keum, H.L., and Sul, W.J. (2023). Bacterial Crosstalk via Antimicrobial Peptides on the Human Skin: Therapeutics from a Sustainable Perspective. J Microbiol *61*, 1-11. 10.1007/s12275-022-00002-8.

10. Burian, M., Wolz, C., and Yazdi, A.S. (2022). Transcriptional adaptation of staphylococci during colonization of the authentic human environment: An overview of transcriptomic changes and their relationship to physiological conditions. Front Cell Infect Microbiol *12*, 1062329. 10.3389/fcimb.2022.1062329.

11. Foster, T.J., Geoghegan, J.A., Ganesh, V.K., and Hook, M. (2014). Adhesion, invasion and evasion: the many functions of the surface proteins of Staphylococcus aureus. Nat Rev Microbiol *12*, 49-62. 10.1038/nrmicro3161.

12. Nakatsuji, T., Chen, T.H., Two, A.M., Chun, K.A., Narala, S., Geha, R.S., Hata, T.R., and Gallo, R.L. (2016). Staphylococcus aureus Exploits Epidermal Barrier Defects in Atopic Dermatitis to Trigger Cytokine Expression. J Invest Dermatol *136*, 2192-2200. 10.1016/j.jid.2016.05.127.

13. da Costa, T.M., Viljoen, A., Towell, A.M., Dufrene, Y.F., and Geoghegan, J.A. (2022). Fibronectin binding protein B binds to loricrin and promotes corneocyte adhesion by Staphylococcus aureus. Nat Commun *13*, 2517. 10.1038/s41467-022-30271-1.

14. Fleury, O.M., McAleer, M.A., Feuillie, C., Formosa-Dague, C., Sansevere, E., Bennett, D.E., Towell, A.M., McLean, W.H.I., Kezic, S., Robinson, D.A., et al. (2017). Clumping Factor B Promotes Adherence of Staphylococcus aureus to Corneocytes in Atopic Dermatitis. Infect Immun *85*. 10.1128/IAI.00994-16.

15. Roy, P., Horswill, A.R., and Fey, P.D. (2021). Glycan-Dependent Corneocyte Adherence of Staphylococcus epidermidis Mediated by the Lectin Subdomain of Aap. mBio *12*, e0290820. 10.1128/mBio.02908-20.

16. Maciag, J.J., Chantraine, C., Mills, K.B., Yadav, R., Yarawsky, A.E., Chaton, C.T., Vinod, D., Fitzkee, N.C., Mathelie-Guinlet, M., Dufrene, Y.F., et al. (2023). Mechanistic basis of staphylococcal interspecies competition for skin colonization. bioRxiv. 10.1101/2023.01.26.525635.

17. Mills, K.B., Roy, P., Kwiecinski, J.M., Fey, P.D., and Horswill, A.R. (2022). Staphylococcal Corneocyte Adhesion: Assay Optimization and Roles of Aap and SasG Adhesins in the Establishment of Healthy Skin Colonization. Microbiol Spectr *10*, e0246922. 10.1128/spectrum.02469-22.

18. Corrigan, R.M., Rigby, D., Handley, P., and Foster, T.J. (2007). The role of Staphylococcus aureus surface protein SasG in adherence and biofilm formation. Microbiology (Reading) *153*, 2435-2446. 10.1099/mic.0.2007/006676-0.

19. Crosby, H.A., Schlievert, P.M., Merriman, J.A., King, J.M., Salgado-Pabon, W., and Horswill, A.R. (2016). The Staphylococcus aureus Global Regulator MgrA Modulates Clumping and Virulence by Controlling Surface Protein Expression. PLoS Pathog *12*, e1005604. 10.1371/journal.ppat.1005604.

20. Yarawsky, A.E., Ori, A.L., English, L.R., Whitten, S.T., and Herr, A.B. (2023). Convergent behavior of extended stalk regions from staphylococcal surface proteins with widely divergent sequence patterns. bioRxiv. 10.1101/2023.01.06.523059.

21. Richard D. Cummings, M.E.E., T.N.C. Ramya, Koichi Kato, Gabriel A. Rabinovich, and Avadhesha Surolia (2022). L-Type Lectins. In Essentials of Glycobiology, A. Varki, R.D. Cummings, J.D. Esko, P. Stanley, G.W. Hart, M. Aebi, D. Mohnen, T. Kinoshita, N.H. Packer, J.H. Prestegard, et al., eds. 10.1101/9781621824213.

22. Severn, M.M., and Horswill, A.R. (2023). Staphylococcus epidermidis and its dual lifestyle in skin health and infection. Nat Rev Microbiol *21*, 97-111. 10.1038/s41579-022-00780-3.

23. Tolo, I., Thomas, J.C., Fischer, R.S.B., Brown, E.L., Gray, B.M., and Robinson, D.A. (2016). Do Staphylococcus epidermidis Genetic Clusters Predict Isolation Sources? J Clin Microbiol *54*, 1711-1719. 10.1128/JCM.03345-15.

24. McCarthy, A.J., and Lindsay, J.A. (2010). Genetic variation in Staphylococcus aureus surface and immune evasion genes is lineage associated: implications for vaccine design and host-pathogen interactions. BMC Microbiol *10*, 173. 10.1186/1471-2180-10-173.

25. Geoghegan, J.A., Corrigan, R.M., Gruszka, D.T., Speziale, P., O'Gara, J.P., Potts, J.R., and Foster, T.J. (2010). Role of surface protein SasG in biofilm formation by Staphylococcus aureus. J Bacteriol *192*, 5663-5673. 10.1128/JB.00628-10.

26. Kuroda, M., Ohta, T., Uchiyama, I., Baba, T., Yuzawa, H., Kobayashi, I., Cui, L., Oguchi, A., Aoki, K., Nagai, Y., et al. (2001). Whole genome sequencing of meticillin-resistant Staphylococcus aureus. Lancet *357*, 1225-1240. 10.1016/s0140-6736(00)04403-2.

27. Bonn, C.M., Rafiqullah, I.M., Crawford, J.A., Qian, Y.M., Guthrie, J.L., Matuszewska, M., Robinson, D.A., and McGavin, M.J. (2023). Repeated Emergence of Variant TetR Family Regulator, FarR, and Increased Resistance to Antimicrobial Unsaturated Fatty Acid among Clonal Complex 5 Methicillin-Resistant Staphylococcus aureus. Antimicrob Agents Chemother *67*, e0074922. 10.1128/aac.00749-22.

28. Challagundla, L., Reyes, J., Rafiqullah, I., Sordelli, D.O., Echaniz-Aviles, G., Velazquez-Meza, M.E., Castillo-Ramirez, S., Fittipaldi, N., Feldgarden, M., Chapman, S.B., et al. (2018). Phylogenomic Classification and the Evolution of Clonal Complex 5 Methicillin-Resistant Staphylococcus aureus in the Western Hemisphere. Front Microbiol *9*, 1901. 10.3389/fmicb.2018.01901.

29. Dabul, A.N., and Camargo, I.L. (2014). Clonal complexes of Staphylococcus aureus: all mixed and together. FEMS Microbiol Lett *351*, 7-8. 10.1111/1574-6968.12358.

30. Bowers, J.R., Driebe, E.M., Albrecht, V., McDougal, L.K., Granade, M., Roe, C.C., Lemmer, D., Rasheed, J.K., Engelthaler, D.M., Keim, P., and Limbago, B.M. (2018). Improved Subtyping of Staphylococcus aureus Clonal Complex 8 Strains Based on Whole-Genome Phylogenetic Analysis. mSphere *3*. 10.1128/mSphere.00464-17.

31. Clark, L.C., Atkin, K.E., Whelan, F., Brentnall, A.S., Harris, G., Towell, A.M., Turkenburg, J.P., Liu, Y., Feizi, T., Griffiths, S.C., Geoghegan, J.A., and Potts, J.R. (2023). Staphylococcal Periscope proteins Aap, SasG, and Pls project noncanonical legume-like lectin adhesin domains from the bacterial surface. J Biol Chem *299*, 102936. 10.1016/j.jbc.2023.102936.

32. Dufrene, Y.F., Ando, T., Garcia, R., Alsteens, D., Martinez-Martin, D., Engel, A., Gerber, C., and Muller, D.J. (2017). Imaging modes of atomic force microscopy for application in molecular and cell biology. Nat Nanotechnol *12*, 295-307. 10.1038/nnano.2017.45.

33. Abdayem, R., Formanek, F., Minondo, A.M., Potter, A., and Haftek, M. (2016). Cell surface glycans in the human stratum corneum: distribution and depth-related changes. Exp Dermatol *25*, 865-871. 10.1111/exd.13070.

34. Danzberger, J., Donovan, M., Rankl, C., Zhu, R., Vicic, S., Baltenneck, C., Enea, R., Hinterdorfer, P., and Luengo, G.S. (2018). Glycan distribution and density in native skin's stratum corneum. Skin Res Technol *24*, 450-458. 10.1111/srt.12453.

35. Dabelsteen, S., Pallesen, E.M.H., Marinova, I.N., Nielsen, M.I., Adamopoulou, M., Romer, T.B., Levann, A., Andersen, M.M., Ye, Z., Thein, D., et al. (2020). Essential Functions of Glycans in Human Epithelia Dissected by a CRISPR-Cas9-Engineered Human Organotypic Skin Model. Dev Cell *54*, 669-684 e667. 10.1016/j.devcel.2020.06.039.

36. Moginger, U., Grunewald, S., Hennig, R., Kuo, C.W., Schirmeister, F., Voth, H., Rapp, E., Khoo, K.H., Seeberger, P.H., Simon, J.C., and Kolarich, D. (2018). Alterations of the Human Skin N- and O-Glycome in Basal Cell Carcinoma and Squamous Cell Carcinoma. Front Oncol *8*, 70. 10.3389/fonc.2018.00070.

37. Tang, L., Chen, X., Zhang, X., Guo, Y., Su, J., Zhang, J., Peng, C., and Chen, X. (2019). N-Glycosylation in progression of skin cancer. Med Oncol *36*, 50. 10.1007/s12032-019-1270-4.

38. Beckwith, D.M., and Cudic, M. (2020). Tumor-associated O-glycans of MUC1: Carriers of the glyco-code and targets for cancer vaccine design. Semin Immunol *47*, 101389. 10.1016/j.smim.2020.101389.

39. Koutsioulis, D., Landry, D., and Guthrie, E.P. (2008). Novel endo-alpha-N-acetylgalactosaminidases with broader substrate specificity. Glycobiology *18*, 799-805. 10.1093/glycob/cwn069.

40. WHO (2022). Report signals increasing resistance to antibiotics in bacterial infections in humans and need for better data.

41. Eyerich, S., Eyerich, K., Traidl-Hoffmann, C., and Biedermann, T. (2018). Cutaneous Barriers and Skin Immunity: Differentiating A Connected Network. Trends Immunol *39*, 315-327. 10.1016/j.it.2018.02.004.

42. Ogonowska, P., Gilaberte, Y., Baranska-Rybak, W., and Nakonieczna, J. (2020). Colonization With Staphylococcus aureus in Atopic Dermatitis Patients: Attempts to Reveal the Unknown. Front Microbiol *11*, 567090. 10.3389/fmicb.2020.567090.

43. Silverberg, J.I. (2017). Public Health Burden and Epidemiology of Atopic Dermatitis. Dermatol Clin *35*, 283-289. 10.1016/j.det.2017.02.002.

44. Avena-Woods, C. (2017). Overview of Atopic Dermatitis. American Journal of Managed Care *23*, S115-S123.

45. Thomas, J.C., Godfrey, P.A., Feldgarden, M., and Robinson, D.A. (2012). Candidate targets of balancing selection in the genome of Staphylococcus aureus. Mol Biol Evol *29*, 1175-1186. 10.1093/molbev/msr286.

710   46.   Sievers, F., Wilm, A., Dineen, D., Gibson, T.J., Karplus, K., Li, W., Lopez, R., McWilliam,
711          H., Remmert, M., Soding, J., Thompson, J.D., and Higgins, D.G. (2011). Fast, scalable
712          generation of high-quality protein multiple sequence alignments using Clustal Omega.
713          Mol Syst Biol *7*, 539. 10.1038/msb.2011.75.
714   47.   Robert, X., and Gouet, P. (2014). Deciphering key features in protein structures with the
715          new ENDscript server. Nucleic Acids Res *42*, W320-324. 10.1093/nar/gku316.
716   48.   Snyder, E.E., Kampanya, N., Lu, J., Nordberg, E.K., Karur, H.R., Shukla, M., Soneja, J.,
717          Tian, Y., Xue, T., Yoo, H., et al. (2007). PATRIC: the VBI PathoSystems Resource
718          Integration Center. Nucleic Acids Res *35*, D401-406. 10.1093/nar/gkl858.
719   49.   Wattam, A.R., Abraham, D., Dalay, O., Disz, T.L., Driscoll, T., Gabbard, J.L., Gillespie,
720          J.J., Gough, R., Hix, D., Kenyon, R., et al. (2014). PATRIC, the bacterial bioinformatics
721          database and analysis resource. Nucleic Acids Res *42*, D581-591. 10.1093/nar/gkt1099.
722   50.   Wattam, A.R., Davis, J.J., Assaf, R., Boisvert, S., Brettin, T., Bun, C., Conrad, N.,
723          Dietrich, E.M., Disz, T., Gabbard, J.L., et al. (2017). Improvements to PATRIC, the all-
724          bacterial Bioinformatics Database and Analysis Resource Center. Nucleic Acids Res *45*,
725          D535-D542. 10.1093/nar/gkw1017.
726   51.   Asnicar, F., Thomas, A.M., Beghini, F., Mengoni, C., Manara, S., Manghi, P., Zhu, Q.,
727          Bolzan, M., Cumbo, F., May, U., et al. (2020). Precise phylogenetic analysis of microbial
728          isolates and genomes from metagenomes using PhyloPhlAn 3.0. Nat Commun *11*,
729          2500. 10.1038/s41467-020-16366-7.
730   52.   Edgar, R.C. (2004). MUSCLE: multiple sequence alignment with high accuracy and high
731          throughput. Nucleic Acids Res *32*, 1792-1797. 10.1093/nar/gkh340.
732   53.   Edgar, R.C. (2004). MUSCLE: a multiple sequence alignment method with reduced time
733          and space complexity. BMC Bioinformatics *5*, 113. 10.1186/1471-2105-5-113.
734   54.   Fu, L., Niu, B., Zhu, Z., Wu, S., and Li, W. (2012). CD-HIT: accelerated for clustering the
735          next-generation sequencing data. Bioinformatics *28*, 3150-3152.
736          10.1093/bioinformatics/bts565.
737   55.   Huang, Y., Niu, B., Gao, Y., Fu, L., and Li, W. (2010). CD-HIT Suite: a web server for
738          clustering and comparing biological sequences. Bioinformatics *26*, 680-682.
739          10.1093/bioinformatics/btq003.
740   56.   Talavera, G., and Castresana, J. (2007). Improvement of phylogenies after removing
741          divergent and ambiguously aligned blocks from protein sequence alignments. Syst Biol
742          *56*, 564-577. 10.1080/10635150701472164.
743   57.   Guindon, S., Dufayard, J.F., Lefort, V., Anisimova, M., Hordijk, W., and Gascuel, O.
744          (2010). New algorithms and methods to estimate maximum-likelihood phylogenies:
745          assessing the performance of PhyML 3.0. Syst Biol *59*, 307-321.
746          10.1093/sysbio/syq010.
747   58.   Maddison, W.P.a.D.R.M. (2021). Mesquite: a modular system for evolutionary analysis.
748   59.   Winn, M.D., Ballard, C.C., Cowtan, K.D., Dodson, E.J., Emsley, P., Evans, P.R.,
749          Keegan, R.M., Krissinel, E.B., Leslie, A.G., McCoy, A., et al. (2011). Overview of the
750          CCP4 suite and current developments. Acta Crystallogr D Biol Crystallogr *67*, 235-242.
751          10.1107/S0907444910045749.
752   60.   Liebschner, D., Afonine, P.V., Baker, M.L., Bunkoczi, G., Chen, V.B., Croll, T.I., Hintze,
753          B., Hung, L.W., Jain, S., McCoy, A.J., et al. (2019). Macromolecular structure
754          determination using X-rays, neutrons and electrons: recent developments in Phenix.
755          Acta Crystallogr D Struct Biol *75*, 861-877. 10.1107/S2059798319011471.
756   61.   Emsley, P., Lohkamp, B., Scott, W.G., and Cowtan, K. (2010). Features and
757          development of Coot. Acta Crystallogr D Biol Crystallogr *66*, 486-501.
758          10.1107/S0907444910007493.
759   62.   Chen, V.B., Arendall, W.B., 3rd, Headd, J.J., Keedy, D.A., Immormino, R.M., Kapral,
760          G.J., Murray, L.W., Richardson, J.S., and Richardson, D.C. (2010). MolProbity: all-atom

761   structure validation for macromolecular crystallography. Acta Crystallogr D Biol
762   Crystallogr *66*, 12-21. 10.1107/S0907444909042073.
763 63. Wang, C., Chantraine, C., Viljoen, A., Herr, A.B., Fey, P.D., Horswill, A.R., Mathelie-
764   Guinlet, M., and Dufrene, Y.F. (2022). The staphylococcal biofilm protein Aap mediates
765   cell-cell adhesion through mechanically distinct homophilic and lectin interactions. PNAS
766   Nexus *1*, pgac278. 10.1093/pnasnexus/pgac278.
767 64. Bechhoefer, J.L.H.a.J. (1993). Calibration of atomic-force microscope tips. Review of
768   Scientific Instruments, 1868-1873. 10.1063/1.1143970.
769 65. Smits, J.P.H., Niehues, H., Rikken, G., van Vlijmen-Willems, I., van de Zande, G.,
770   Zeeuwen, P., Schalkwijk, J., and van den Bogaard, E.H. (2017). Immortalized N/TERT
771   keratinocytes as an alternative cell source in 3D human epidermal models. Sci Rep *7*,
772   11838. 10.1038/s41598-017-12041-y.

773

## Acknowledgements

**Declaration of interests**

A.B.H. has served as a Scientific Advisory Board member for Hoth Therapeutics, Inc., holds equity in Hoth Therapeutics and Chelexa BioSciences, LLC, and was a co-inventor on seven patents broadly related to the subject matter of this work.

30

## Figure legends

**Figure 1. SasG Variation in the context of *S. aureus* phylogenetic diversity.** (**A**) Maximum likelihood phylogenetic tree of 574 *S. aureus* isolates based on their proteome. For each isolate, SasG status is mapped to ring 1, SasG type (defined in Panel B) is mapped to ring 2, SasG B-repeat number is mapped to ring 3, and the clonal complex of the isolate is mapped to ring 4. (**B**) Histograms of SasG B-repeats from both SasG allelic types. (**C**) Maximum likelihood phylogenetic tree of SasG from 191 aligned full-length sequences identifies two SasG allelic types.

**Figure 2. The SasG-II lectin contains a unique non-aromatic residue in the glycan binding pocket.** (**A**) Crystal structure of the SasG-II lectin showing the structural $Ca^{2+}$ ion, the conserved central D241 residue that adopts an atypical *trans* conformation, and the side chains of S392, R394, and Q395 near the end of β17. (**B**) Comparative view of SasG-II in the same orientation. Residues R391 and W392 are analogous to R394 and Q395 in SasG-II; note the distinct positioning of corresponding residues W392 (SasG-II) and Q395 (SasG-I). (**C**) Close-up view of the region near the end of β17, rotated by approximately 45° from panels A and B. Note the sharp bend of the main chain near R391 in SasG-I that is not observed in SasG-II. (**D**) Surface view of SasG-II showing the putative binding pocket lacking an aromatic residue at its base.

**Figure 3. Multiparametric nanoimaging using single bacterial probes indicates SasG-II binds a broader variety of ligands than SasG-I**. (**A**) Height images (top) and adhesion images (bottom) of corneocytes recorded in PBS using a SasG-II, SasG-I, or EV (SasG[-]) cell probe. See also Figure S2-S4. (**B**) Histograms of adhesion forces registered on whole corneocytes (total of n = 9,590 curves for one representative SasG-II probe; n = 2,532 curves for one representative SasGI probe). The arrow at the top left of the histograms stands for the

31

813    non-adhesive events.  (**C**) Box plot comparing adhesion probabilities for SasG-II (n = 4 from 3

814    independent bacterial cultures), SasG-I (n = 4 from 2 independent bacterial cultures), SasG(-) (n

815    = 4 from 2 independent bacterial cultures) or colloidal (n = 2) probes. For more data, see

816    Figures S1, S2, and S3.

817

818    **Figure 4. SasG-I and -II mediated adhesion to corneocytes shows differential responses**

819    **upon treatment with glycosidases.** *S. carnosus-sasG*$_{COL}$ (SasG-I) and *S. carnosus-sasG*$_{MW2}$

820    (SasG-II) were tested for adhesion to corneocytes following pre-incubation with (**A**) PNGase F,

821    (**B**) O-Glycosidase, (**C**) α1-2,3,6 Mannosidase, (**D**) α1-3,4 Fucosidase, (**E**) β-*N*-

822    Acetylglucosaminidase S, (**F**) β1-4 Galactosidase S, and (**G**) α2-3,6,8 Neuraminidase. The

823    percent area of adhesion in 10 images from three independent experiments (n = 30) was

824    measured with Fiji ImageJ and analyzed in GraphPad Prism. Statistical significance was

825    analyzed using the unpaired t-test or non-parametric Mann-Whitney test for data with non-

826    normal distribution (****$P<0.0001$).

827

828    **Figure 5. SasG-II-mediated adhesion is mediated by the lectin subdomain and may bind**

829    **the same ligand as Aap and SasG-I.** (**A**) MRSA MW2 (SasG-II) was tested for adhesion to

830    healthy human corneocytes after pre-incubation/blocking with 5 μM of purified lectins. MRSA

831    MW2 Δ*sasG* was used as a negative control strain. **$P=0.0019$. (**C**) SasG-II-expressing *S.*

832    *carnosus-sasG*$_{MW2}$ was tested for adhesion to healthy human corneocytes after pre-

833    incubation/blocking with 5 μM of purified lectins. *S. carnosus*-pALC2073 EV was used as a

834    negative control strain. *S. epidermidis* Δ*ica* was tested for adhesion to corneocytes following

835    pre-incubation/blocking with 100 μg/mL of purified full-length or A-domain SasG-II. *S.*

836    *epidermidis* Δ*ica* Δ*aap* was used as a negative control strain. (**G**) SasG-I-expressing *S.*

837    *carnosus-sasG*<sub>COL</sub> was tested for adhesion to healthy human corneocytes after pre-

838    incubation/blocking with 100 µg/mL of purified full-length or A-domain SasG-II. *S. carnosus*-

839    pALC2073 EV was used as a negative control strain. **$P$=0.0091. (**B, D, F, H**) Representative

840    bright-field (representing corneocytes) and green-channel (representing GFP-expressing

841    bacteria) overlay microscopy images of experimental groups tested in Panels A, C, E, and G,

842    respectively. (**All panels**) The percent area of adhesion in 10 images from three independent

843    experiments (n = 30) was measured with Fiji ImageJ and analyzed in GraphPad Prism.

844    Statistical significance was analyzed using ordinary one-way ANOVA (***$P$=0.0002*;

845    ****$P$<0.0001).

846

847    **Figure 6. SasG-I and SasG-II-mediated adhesion to differentiated N/TERT keratinocytes**

848    **following treatment with glycosidases suggests complex N-linked glycans and core 2 O-**

849    **glycans may be important for SasG-I and SasG-II binding.** *S. carnosus*-pALC2073 EV,

850    SasG-I-expressing *S. carnosus-sasG*<sub>COL</sub> and SasG-II-expressing *S. carnosus-sasG*<sub>MW2</sub>, and

851    SasG-II-expressing *S. carnosus* with the A-domain deleted (*S. carnosus-sasG*<sub>MW2ΔA</sub>) at an MOI

852    of 5 were tested for adhesion to either differentiated (**A and B**) or undifferentiated (**C and D**)

853    N/TERT keratinocytes. (**A**) Adhesion to terminally differentiated cells as shown by overall

854    percent adhesion. (**B**) Adhesion to terminally differentiated cells as shown by percent cell

855    association to pALC2073-*sasG*<sub>MW2</sub> input inoculum. Both SasG-expressing strains adhered more

856    to differentiated cells than the EV and A domain mutant controls. (**C**) Adhesion to a monolayer

857    of undifferentiated cells as shown by overall percent adhesion. (**D**) Adhesion to a monolayer of

858    undifferentiated cells as shown by percent cell association to pALC2073-*sasG*<sub>MW2</sub> input

859    inoculum. There were no significant differences in adhesion between the EV and A domain

860    mutant controls and the SasG-expressing strains. (**A-D**) The CFU/mL of three independent

861    experiments (n = 3) were calculated and analyzed for statistical significance in GraphPad Prism

862    using ordinary one-way ANOVA. (**E**) Data from panels A and C displaying differences in

863    adhesion between differentiated and undifferentiated N/TERT keratinocytes for SasG-I-

864    expressing *S. carnosus-sasG*$_{COL}$ and SasG-II-expressing *S. carnosus-sasG*$_{MW2}$. Both strains

865    adhered well to differentiated N/TERT keratinocytes, and did not adhere well to undifferentiated

866    N/TERT keratinocytes. No statistical analyses were performed for Panel E. SasG-I-expressing

867    *S. carnosus-sasG*$_{COL}$ and SasG-II-expressing *S. carnosus-sasG*$_{MW2}$ were tested for overall

868    percent adhesion to differentiated N/TERT keratinocytes following treatment with (**F**) β-*N*-

869    Acetylglucosaminidase S and (**G**) β1-4 Galactosidase S. β1-4 Galactosidase S reduced

870    adhesion of both strains, while β-*N*-Acetylglucosaminidase S resulted in a greater reduction in

871    adhesion of *S. carnosus-sasG*$_{MW2}$. The CFU/mL of three independent experiments (n = 3) were

872    calculated and analyzed for statistical significance in GraphPad Prism using an unpaired t-test.

873    *\*P*=0.0500.

874

875    **Figure 7. Model for SasG-I and SasG-II-mediated adhesion to healthy human skin**

876    **corneocytes.** SasG-I blocks adhesion of SasG-II, and likewise SasG-II can block adhesion of

877    SasG-I, indicating they can all bind the same corneocyte receptor in some capacity. However,

878    removal of N-glycans and core 1 or 3 O-glycans does not block SasG-II binding as it does with

879    SasG-I, suggesting that SasG-II may bind a core 2 O-glycan structure elsewhere on the
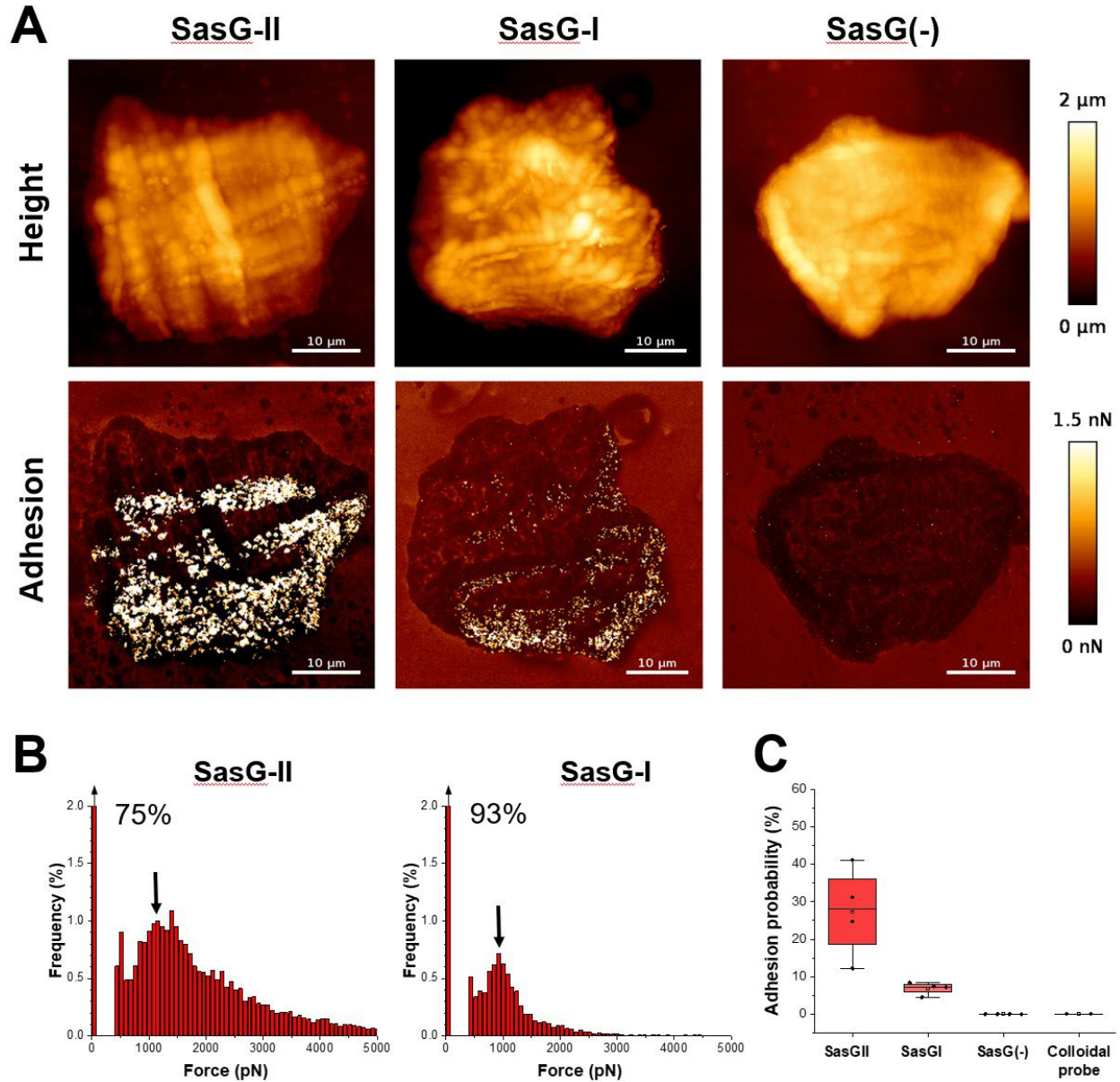
880    corneocyte receptor.

881
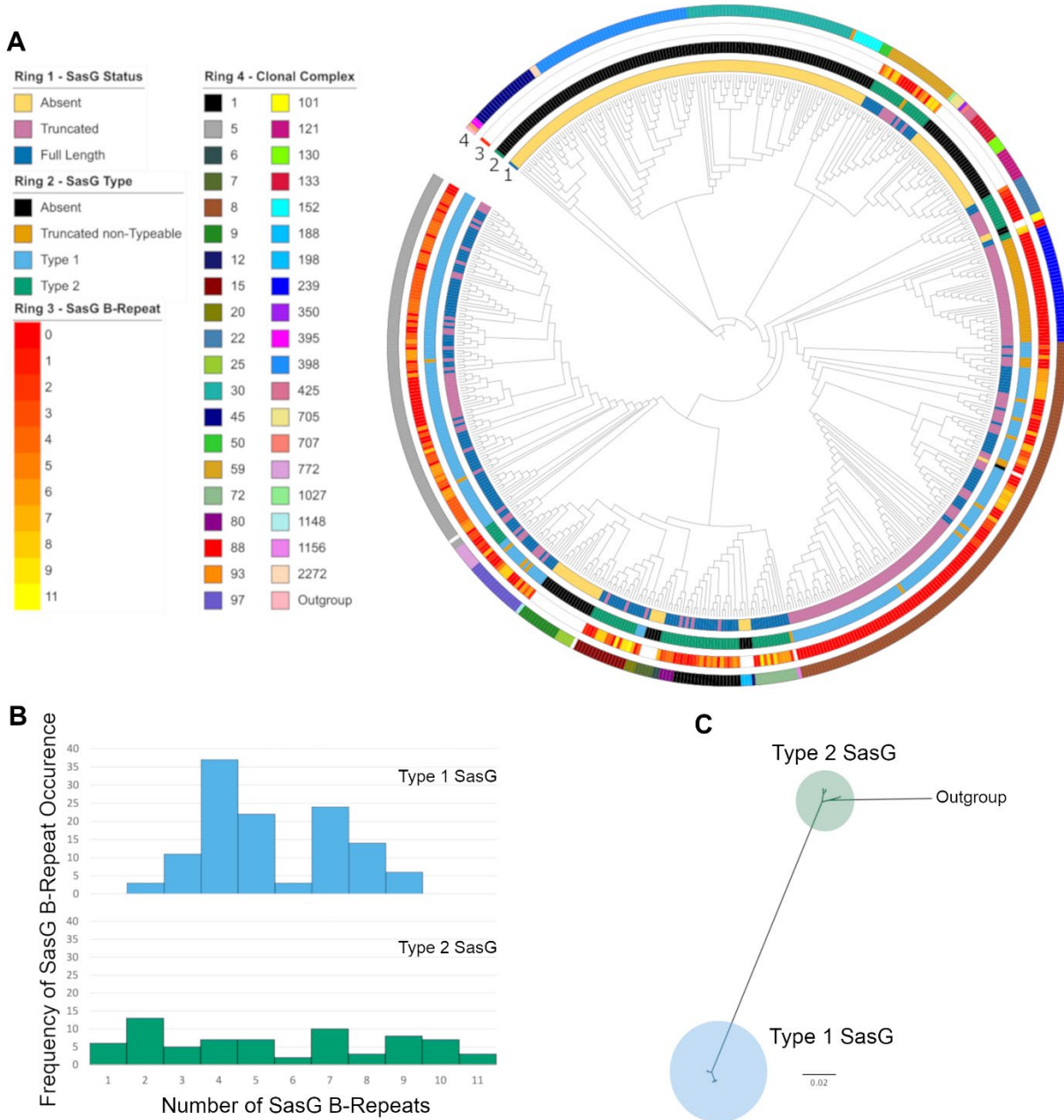
**Figure 1. SasG Variation in the context of *S. aureus* phylogenetic diversity.**
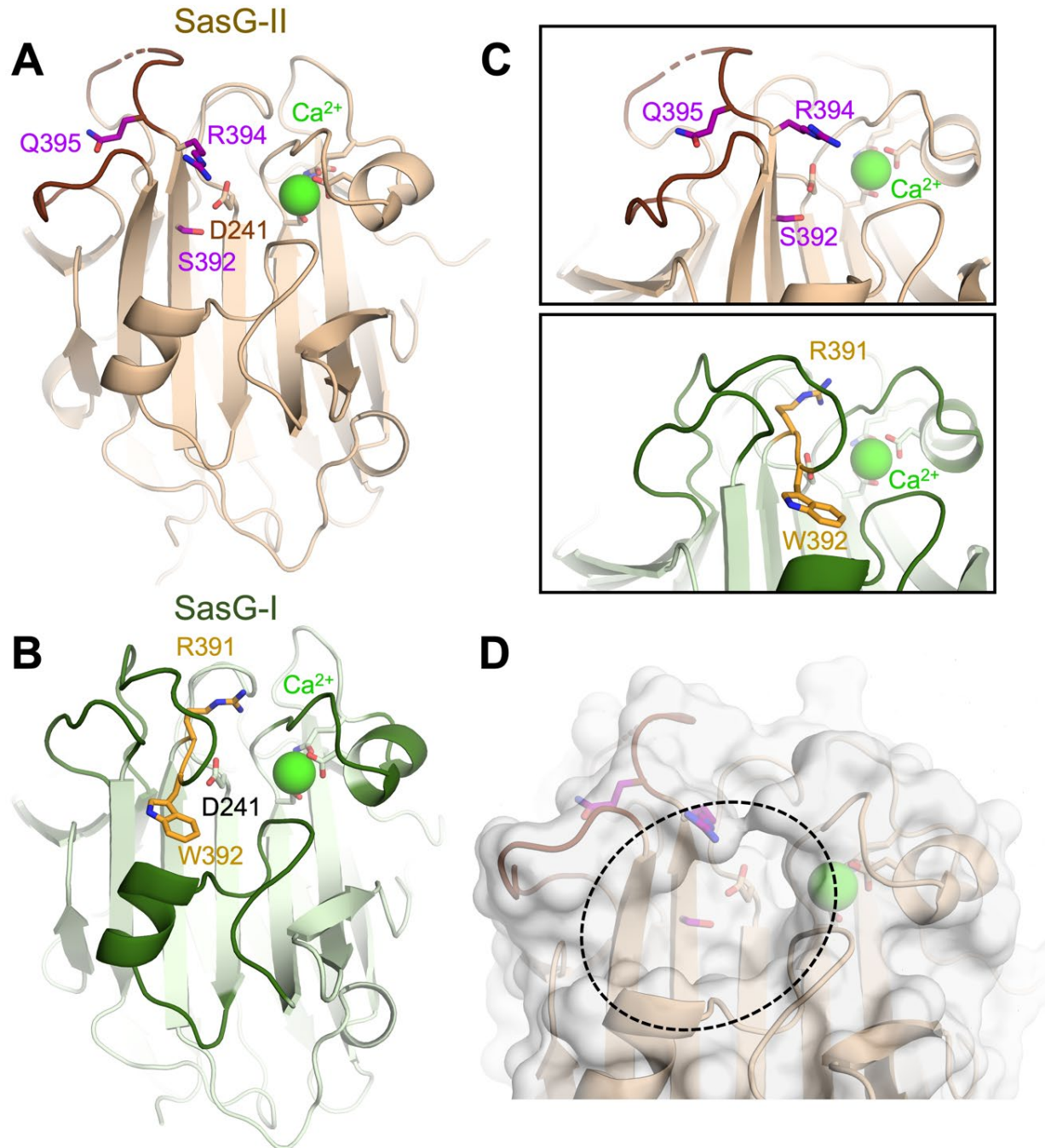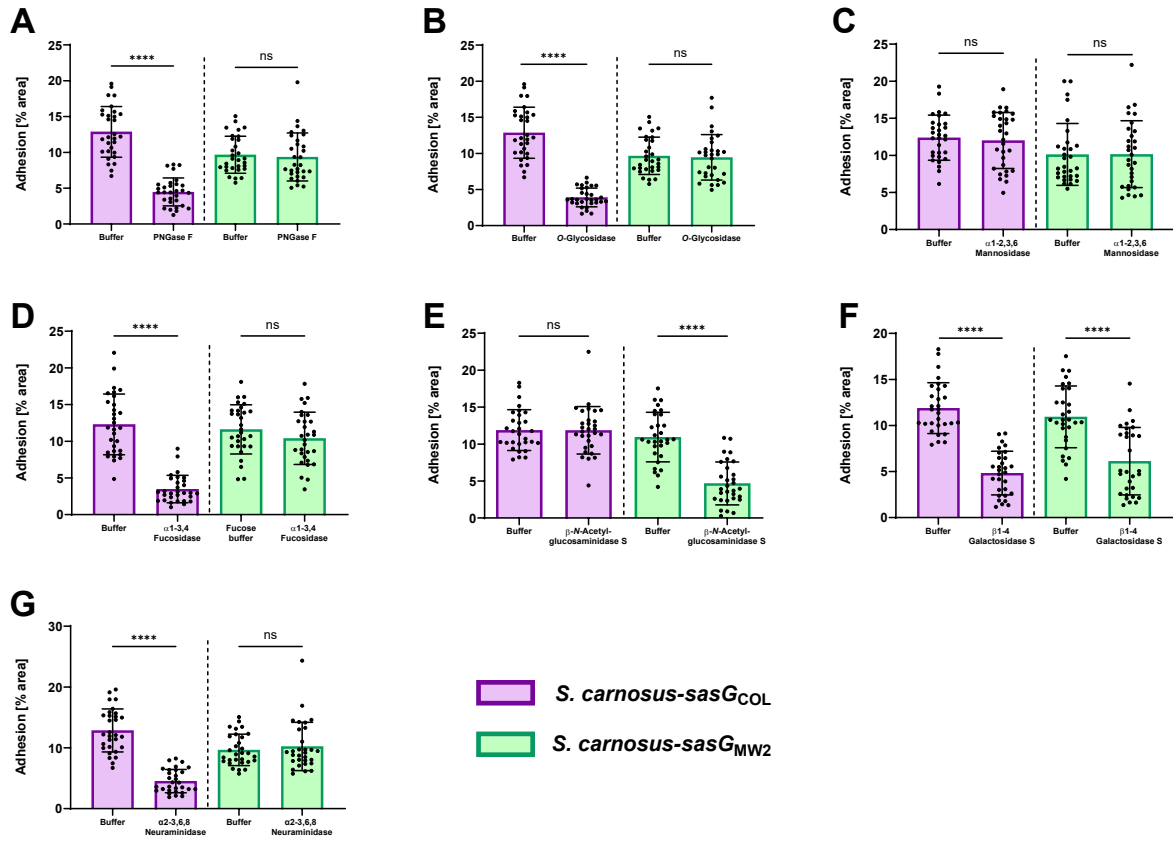
**Figure 2. The SasG-II lectin contains a unique non-aromatic residue in the glycan binding pocket.**
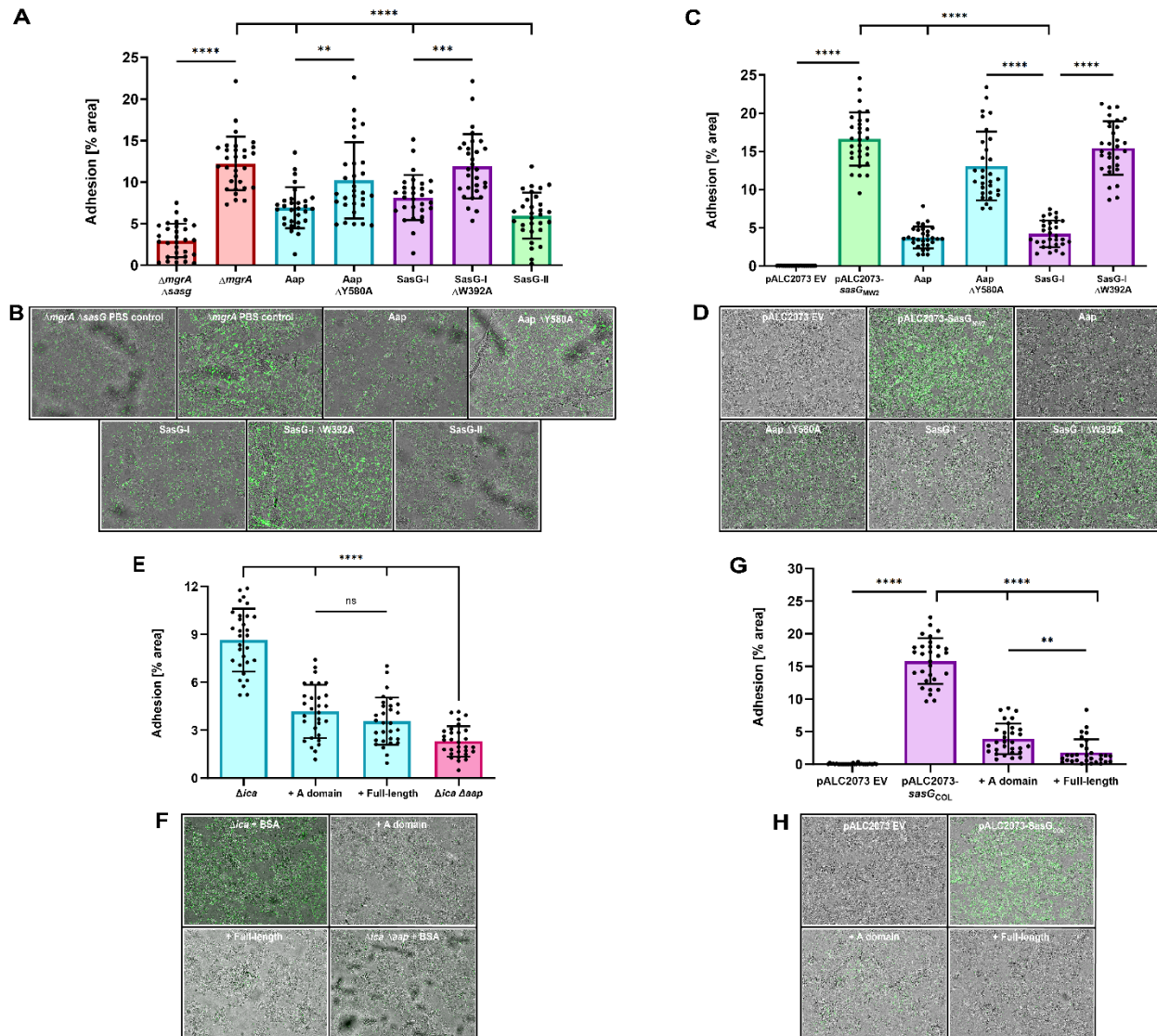
**Figure 3. Multiparametric nanoimaging using single bacterial probes indicates SasG-II binds a broader variety of ligands than SasG-I**

**Figure 4. SasG-I and -II mediated adhesion to corneocytes shows differential responses upon treatment with glycosidases.**
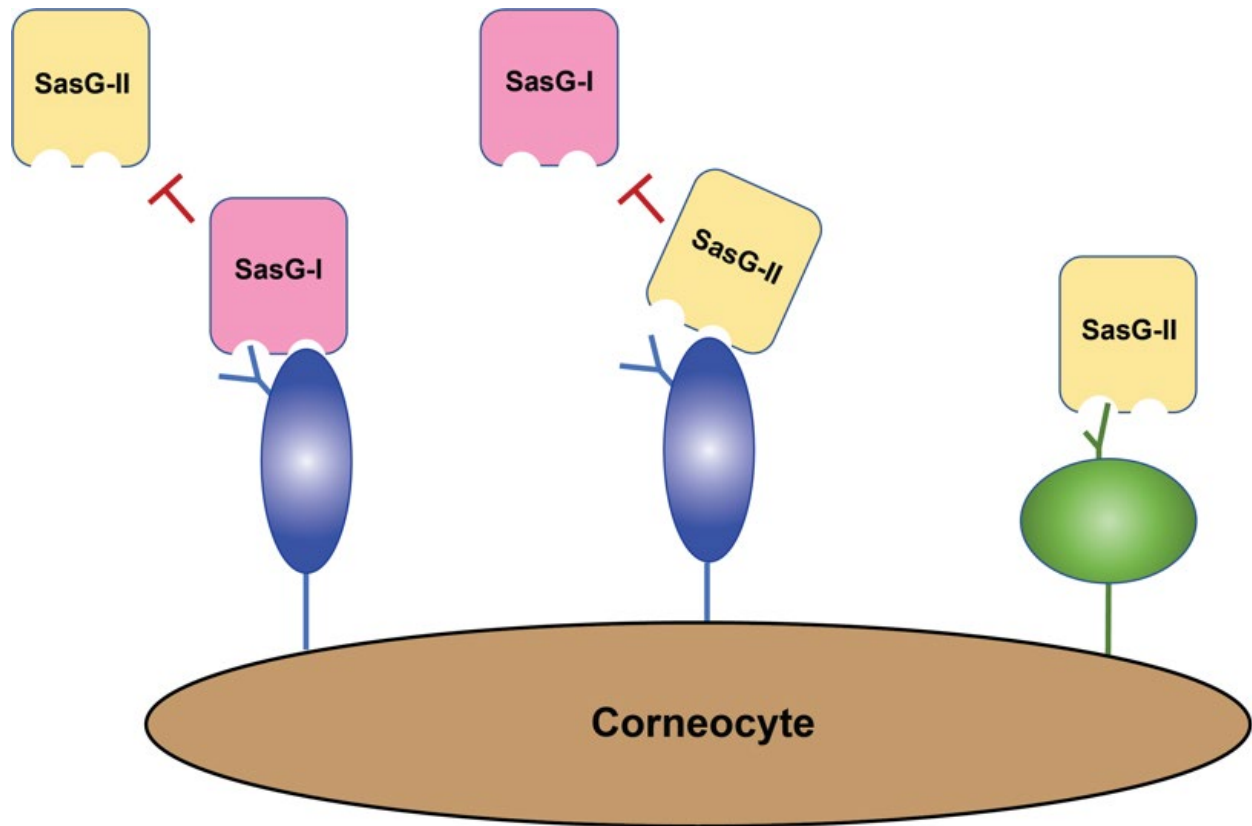
**Figure 5. SasG-II-mediated adhesion is mediated by the lectin subdomain and may bind the same ligand as Aap and SasG-I.**
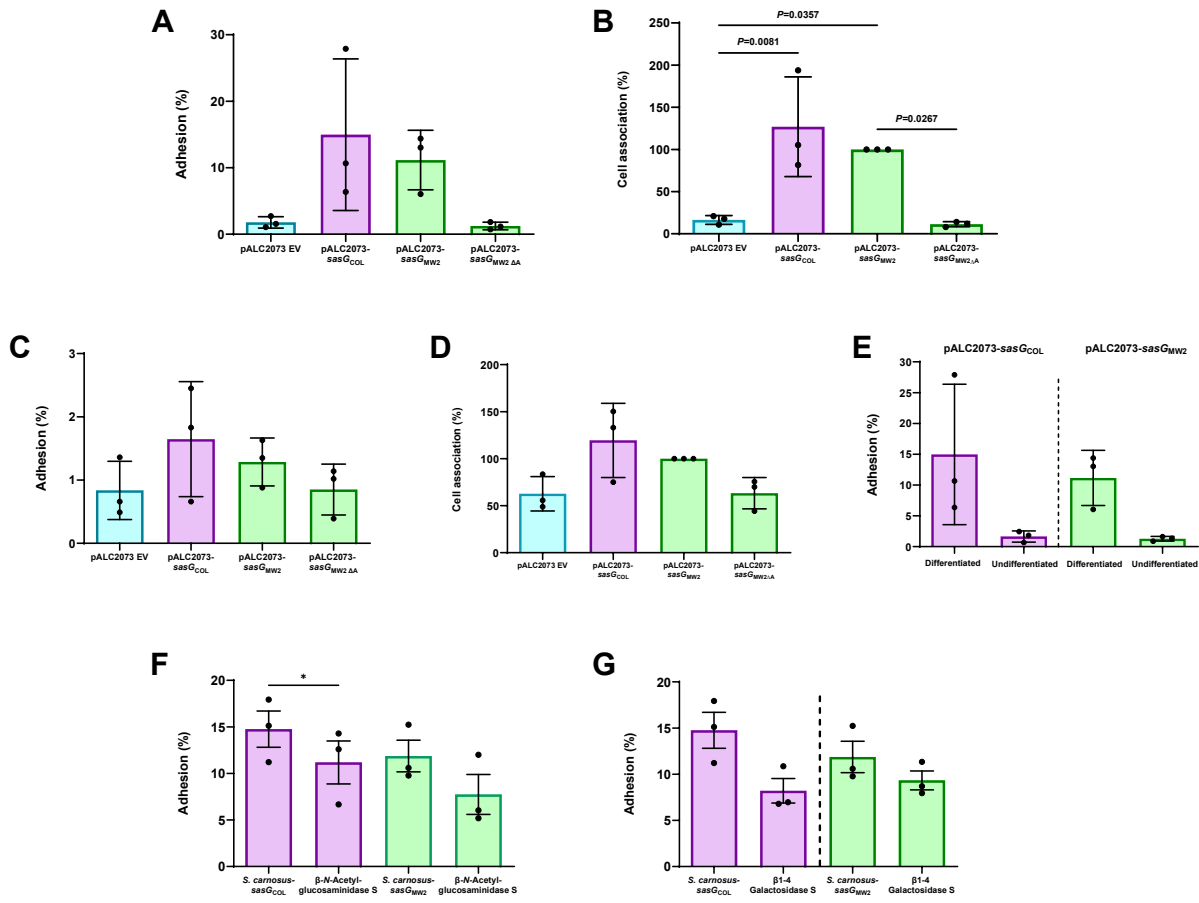
**Figure 6. SasG-I and SasG-II-mediated adhesion to differentiated N/TERT keratinocytes following treatment with glycosidases suggests complex N-linked glycans and core 2 O-glycans may be important for SasG-I and SasG-II binding.**

**Figure 7. Model for SasG-I and SasG-II-mediated adhesion to healthy human skin corneocytes.**